

# Spindle Oscillations during Asymmetric Cell Division Require a Threshold Number of Active Cortical Force Generators

Jacques Pecreaux, Jens-Christian Röper, Karsten Kruse, Frank Jülicher, Anthony A. Hyman, Stephan W. Grill, and Jonathon Howard

## Supplemental Experimental Procedures

### Culture Conditions, RNA-Mediated Interference, Western Blots, and Spindle Severing

Nematode strains expressing  $\gamma$ -tubulin-GFP [S1] were grown at 16°C, and embryos were mounted and imaged at  $23 \pm 0.5^\circ\text{C}$  (unless otherwise stated) as described earlier [S2]. For RNAi of *gpr-1* and *gpr-2* (genes C38C10.4 and F22B7.13, which are >97% identical in sequence and thus indistinguishable by RNAi), young adults were injected with dsRNA derived from genomic DNA obtained by using the PCR primers 5'-AATTAACCTCACTAAAGGTCTGGCAGCAGA CAGTTCAG-3' and 5'-TAATACGACTCACTATAGGAGCATGTGATT CCACACGTC-3' [S3]. Injected worms were kept at 24.5°C, and embryos were analyzed between 2 hr and 42 hr after injection. For RNAi of the dynein-light-intermediate-chain gene, *dli-1* (C39E9.14), young adult hermaphrodites were transferred onto feeding plates containing the bacterial strain for *dli-1* inactivation obtained from Geneservice [S4], as described elsewhere [S5, S6], and left at 24.5°C for different times before observation. Western blots were performed as described previously [S7], with 50 worms in each condition (control and 10, 20, 30, and 40 hr after injection or transfer). Severing of the central spindle at different times after injection was performed as described [S8], with a pulsed UV laser ( $\lambda = 355$  nm, 400 ps, 20  $\mu\text{J}$ /pulse, PowerChip, JDS Uniphase) [S9].

### Automatic Spindle-Pole Tracking

The positions of both spindle poles were tracked at 2 frames/s with a precision of  $\sim 100$  nm by using the following procedure. First, the image was low-pass-filtered at a spatial frequency of  $1.125 \mu\text{m}^{-1}$ . Second, a correlation was computed between the filtered image and a difference-of-Gaussians model image. Third, the centrosome position was computed by using a center-of-gravity algorithm applied to the result of the correlation. The maximum amplitude of an oscillation was defined as one half of the peak-to-peak variation in the spindle-position trace after it was passed through a band-pass filter with lower and upper cutoff frequencies of 10 and 100 mHz, respectively. The contour of the embryo was obtained from the cytoplasmic fluorescence, and the position the spindle within the cell was calculated as the mean position of the two spindle poles. Four frequency measurements were made during each period of an oscillation by measuring the times in the cycle at which the position and

velocity were at an extremum. Analysis was performed with MatLab (The MathWorks). Values are mean  $\pm$  SD unless otherwise stated.

### Simulations

Equation S1 was solved numerically in MatLab.  $k_{\text{off}}$  was varied with time as shown in Box 1, Figure 1A; this in turn makes the coefficients in Equation S1 vary with time (Equations S2 and S3). Because spontaneous oscillations build up from fluctuations, noise was added in each simulation step. The noise,  $\eta(t)$ , was added at each time step and was constructed in such a way that it corresponded to continuous time noise with the following properties:  $\langle \eta(t) \rangle = 0$  and  $\langle \eta(0)\eta(t) \rangle = 2kT\gamma\delta(t)$ , where  $kT$  is the Boltzmann constant times absolute temperature,  $\gamma = 39$  mN·s/m corresponds to a damping term arising from fluctuations of the motors [S10] and gives a noise amplitude somewhat smaller than the measured noise (compare Figure 1C with Figure 5E), and  $\delta(t)$  is the Dirac delta function. The parameters used in the simulation are stated in the legend to Figure 5.

### The Antagonistic-Motors Model

Because each spindle pole oscillates even after the spindle has been bisected with a UV laser [S8], we treat the oscillations of the two spindle poles separately (Box 1, Figure 1A). The cortical force generators are postulated to be protein complexes that contain one or more motor proteins. A motor protein binds near the plus end of an astral microtubule and moves processively toward the minus end, generating a force that pulls the spindle pole toward the cortex. The force has components parallel to and perpendicular to the AP axis as shown in Box 1, Figure 1A. In one picture, the force-generating complex is acting as a depolymerase in the sense that the net result is a decrease in length of the astral microtubules. Alternatively, the microtubule may not depolymerize and instead is bent along the cortex. The model is general enough to incorporate both pictures.

The motors obey a “force-velocity” curve whereby the speed,  $v$ , of a motor toward the minus end of the microtubule decreases as the load force,  $f$ , is increased. If the speed is low ( $|v| \ll v_m$ , where  $v_m$  is the maximum speed), in what has been termed the “force-limited” regime [S9], we can write  $f \approx \bar{f} - f'v$ , where  $\bar{f}$  is the “stall” or “reversal force” above which the motor reverses direction and  $f'$  is the slope of the force-velocity curve at the reversal force. The existence of a reversal force was recently demonstrated experimentally for kinesin [S11]. The numerical value of  $f'$  is on the order of  $\bar{f}/v_m$ . The maximum speed is on the order of  $2 \mu\text{m/s}$ , the highest speed of any of the

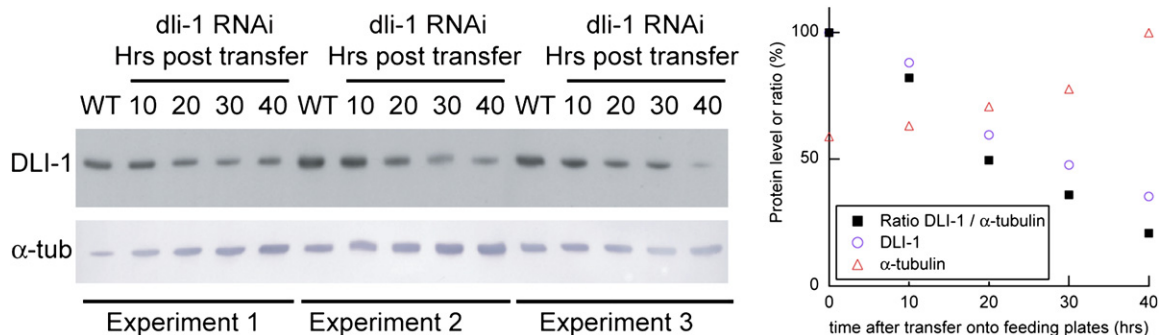


Figure S1. Western Blot and Quantification of DLI-1 Rundown

The left panel is a western blot for three experiments showing the dynein light intermediate chain (DLI-1) protein levels at the indicated times after transfer to the feeding plates. WT denotes uninjected control. Also shown are the  $\alpha$ -tubulin protein levels, which serve as loading controls. The right panel shows the average protein levels for the three experiments normalized to the highest level: The DLI-1 levels decrease, as do their ratios relative to the tubulin control.

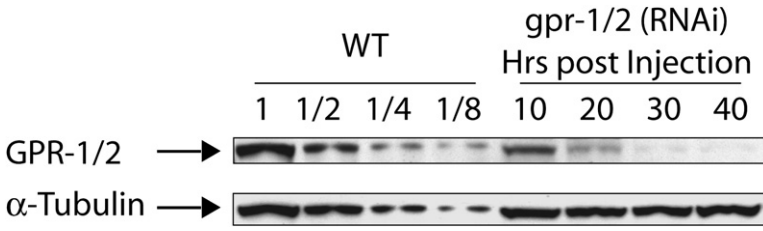


Figure S2. Western Blot of GPR-1/2 Run-down

Western blot showing the change in GPR-1/2 protein levels at the indicated times after the injection of dsRNA. WT denotes uninjected controls at the indicated dilution. Also shown are the  $\alpha$ -tubulin protein levels, which serve as loading controls. These data are quantified in Figure 3A in the main text.

centrosomal fragments [S9], and is consistent with the speed of cytoplasmic dynein [S12]. We take  $\bar{f} = 6$  pN, the stall force of kinesin and cytoplasmic dynein [S13]. We take  $f' = 3 \mu\text{N}\cdot\text{s}/\text{m}$ .

If we represent the position of the spindle by  $y$  and its velocity and higher time derivatives by  $\dot{y}$  and  $\ddot{y}$ , etc., then we can express the force generated by a motor on the upper cortex by

$$f_+ \approx \bar{f} - f'\dot{y} \quad (\text{S1})$$

In the following we derive a linear solution to the model; the full nonlinear solution is in [S14]. The linear equations are good approximations provided that the oscillations are small because the symmetry of the spindle about the AP axis ensures that the second-order terms ( $\dot{y}^2, \ddot{y}^2, \dot{y}\ddot{y}$ ) cancel out.

The motor forces, which pull the spindle pole away from the AP axis, are opposed by a centering process. This process, whose existence is inferred from the observation that the spindle is centered prior to anaphase onset (i.e., before the cortical force generators are turned on), exerts a force on the spindle pole that increases with the displacement from the AP axis. Such a force-displacement relationship defines a spring, and we assume that it is Hookean with a spring constant  $K$ . The molecular substrate for this “centering spring” could be the pushing or pulling of microtubules that contact the cortex at sites distinct from the motors [S15, S16]. If buckling microtubules contribute to centering, then the value of  $K$  is  $\sim 10 \mu\text{N}/\text{m}$  (Equation 3 in [S15], assuming that the number of microtubules contributing to centering,  $Np$ , is 100).

The movement of the spindle pole is expected to be opposed by drag forces that arise from viscosity of the ooplasm [S17] as well as the dynamic rearrangements of the microtubules themselves [S15]. We assume that the drag force is proportional to the velocity, with drag coefficient  $\Gamma$ . If the viscosity of the cytoplasm is 100–1000 times larger than that of an aqueous solution [S17], then the drag is on the order of  $100 \mu\text{N}\cdot\text{s}/\text{m}$ . If the damping is due to the dynamics of buckling microtubules, then  $\Gamma$  is again on this order of  $100 \mu\text{N}\cdot\text{s}/\text{m}$  (Equation 10 in [S15], assuming that the time for microtubules to grow from the pole to the cortex,  $\tau^*$ , is 20 s [S18]).

The spindle pole together with its astral microtubules is equivalent to the mechanical circuit shown in Box 1, Figure 1B (right). The activity of the motors depends on the net forces that act on them as explained in the next paragraph.

The motors are processive, meaning that they take many steps before dissociating. This implies that a change in the probability that the motor is attached,  $p$ , lags behind a change in the load force according to  $\dot{p}(t) = -k_{\text{off}}p + k_{\text{on}}(1-p)$ , where  $k_{\text{on}}$  and  $k_{\text{off}}$  are the on and off rates for the motor binding to a microtubule. The off rate is assumed to increase exponentially with load as observed experimentally for kinesin [S19]:  $k_{\text{off}}(f) = k_0 \exp(f/f_c) \approx \bar{k}_{\text{off}}(1 - f'\dot{y}/f_c)$ , where we have substituted the force-velocity relation and assumed that the speed is low.  $\bar{k}_{\text{off}} = k_{\text{off}}(\bar{f})$ . We take  $f_c = 1.5$  pN. This is somewhat smaller than the value of 4 pN for kinesin-microtubule detachment and the 4–5 pN for cadherin-cadherin detachment [S20]. The on rate of  $0.6 \text{ s}^{-1}$  is chosen to give the correct frequency of oscillation.

The equation of motion of the spindle pole is

$$\Gamma\dot{y} + Ky = F_+ + F_- \quad (\text{S2})$$

$F_+$  is the force generated by the motors on the upper side of the cortex, and  $F_-$  is the force generated by the motors on the lower side. The upper cortical force is given by

$$F_+ = Np_+f_+ \quad (\text{S3})$$

[S9], where  $N$  is the number of motors,  $p_+$  is the probability of an upper motor being attached, and  $f_+$  is the single-motor force

generated by an upper motor. An analogous expression holds for the lower cortex. We can express the attached probability at the upper cortex as

$$\dot{p}_+ \approx -\frac{1}{\bar{\tau}} \left[ 1 - \frac{f'}{f_c}(1 - \bar{p})\dot{y} \right] p_+ + k_{\text{on}}, \quad (\text{S4})$$

where  $\bar{\tau} = (k_{\text{on}} + \bar{k}_{\text{off}})^{-1}$  is the delay in the response of the motors to changing forces and  $\bar{p} = k_{\text{on}}/(k_{\text{on}} + \bar{k}_{\text{off}})$  is the mean attached probability of the motors (which reflects their activity as defined in the text). If the delay is short (on the order of 1 s) compared to the period of spindle oscillation ( $\sim 20$  s), then the speed changes little over time ( $|\dot{y}| \ll |\ddot{y}|/\bar{\tau}$ ). In this case, the probability can be expressed to linear order as:

$$p_+ \approx \bar{p} + \frac{f'}{f_c}\bar{p}(1 - \bar{p})\dot{y} - \frac{f'}{f_c}\bar{p}(1 - \bar{p})\ddot{y}. \quad (\text{S5})$$

This can be checked by substituting S5 (and its derivative) back into Equation S4 and comparing the lowest-order terms. The attached probability lags the velocity by the time  $\bar{\tau}$ .

The symmetry of the spindle implies that  $f_-(\dot{y}) = -f_+(-\dot{y})$  and  $p_-(\dot{y}, \ddot{y}) = p_+(-\dot{y}, -\ddot{y})$ . Substituting the force-velocity curve (Equation S1) and  $F_- = Np_-f_-$  into S2, and using S5 and the symmetry relations, we obtain the following equation of motion:

$$\Gamma\ddot{y} + (\Gamma - \Xi)\dot{y} + Ky = 0. \quad (\text{S6})$$

This equation corresponds to the mechanical circuit shown in Box 1, Figure 1B (left).  $\Gamma$  and  $\Xi$  are given by

$$\begin{aligned} \Gamma &= 2N \left\{ \frac{\bar{f}}{f_c} \bar{p}(1 - \bar{p}) \right\} f' \bar{\tau} \\ \Xi &= 2N \left\{ \frac{\bar{f}}{f_c} \bar{p} \left[ (1 - \bar{p}) - \frac{f_c}{\bar{f}} \right] \right\} f'. \end{aligned} \quad (\text{S7})$$

$\Gamma$  has units of mass and corresponds to a chemomechanical “inertia.”  $\Xi$  has units of damping, but if it is positive, it gives rise to a force in the same direction as the velocity; we therefore call it “negative damping” to distinguish it from positive damping, where the force opposes the velocity. For fixed  $k_{\text{on}}$ ,  $\Gamma$  is maximum when  $\bar{p} = 2/3$  (noting that  $\bar{\tau} = \bar{p}/k_{\text{on}}$ ), whereas for fixed  $\bar{k}_{\text{off}}$  it has a maximum when  $\bar{p} = 1/3$  [noting that  $\bar{\tau} = (1 - \bar{p})/\bar{k}_{\text{off}}$ ] as shown in Figure 5D.

If the negative damping ( $\Xi$ ) exceeds a threshold set by the passive damping ( $\Gamma$ ) (i.e.,  $\Xi > \Gamma$ ), then the total damping is negative. In this case, there is positive feedback and the system described by Equation S1 becomes unstable and begins to oscillate. Close to the instability, the oscillation frequency is

$$\omega_0 \approx \sqrt{K/\Gamma} \text{ rad/s}. \quad (\text{S8})$$

If the negative damping falls below the passive damping, then the system is stable and the oscillations die out exponentially.

## Supplemental References

- S1. Oegema, K., Desai, A., Rybina, S., Kirkham, M., and Hyman, A.A. (2001). Functional analysis of kinetochore assembly in *Caenorhabditis elegans*. *J. Cell Biol.* **153**, 1209–1226.
- S2. Gonczy, P., Schnabel, H., Kaletta, T., Amores, A.D., Hyman, T., and Schnabel, R. (1999). Dissection of cell division processes in the one cell stage *Caenorhabditis elegans* embryo by mutational analysis. *J. Cell Biol.* **144**, 927–946.
- S3. Gonczy, P., Echeverri, C., Oegema, K., Coulson, A., Jones, S.J., Copley, R.R., Duperon, J., Oegema, J., Brehm, M., Cassin,

- E., et al. (2000). Functional genomic analysis of cell division in *C. elegans* using RNAi of genes on chromosome III. *Nature* *408*, 331–336.
- S4. Kamath, R.S., and Ahringer, J. (2003). Genome-wide RNAi screening in *Caenorhabditis elegans*. *Methods* *30*, 313–321.
- S5. Fraser, A.G., Kamath, R.S., Zipperlen, P., Martinez-Campos, M., Sohrmann, M., and Ahringer, J. (2000). Functional genomic analysis of *C. elegans* chromosome I by systematic RNA interference. *Nature* *408*, 325–330.
- S6. Kamath, R.S., Martinez-Campos, M., Zipperlen, P., Fraser, A.G., and Ahringer, J. (2001). Effectiveness of specific RNA-mediated interference through ingested double-stranded RNA in *Caenorhabditis elegans*. *Genome Biol.* *2*. RESEARCH0002. Published online December 20, 2000. 10.1186/gb-2000-2-1-research0002.
- S7. Ozlu, N., Srayko, M., Kinoshita, K., Habermann, B., O'Toole, E.T., Muller-Reichert, T., Schmalz, N., Desai, A., and Hyman, A.A. (2005). An essential function of the *C. elegans* ortholog of TPX2 is to localize activated aurora A kinase to mitotic spindles. *Dev. Cell* *9*, 237–248.
- S8. Grill, S.W., Gonczy, P., Stelzer, E.H., and Hyman, A.A. (2001). Polarity controls forces governing asymmetric spindle positioning in the *Caenorhabditis elegans* embryo. *Nature* *409*, 630–633.
- S9. Grill, S.W., Howard, J., Schaffer, E., Stelzer, E.H., and Hyman, A.A. (2003). The distribution of active force generators controls mitotic spindle position. *Science* *301*, 518–521.
- S10. Nadrowski, B., Martin, P., and Julicher, F. (2004). Active hair-bundle motility harnesses noise to operate near an optimum of mechanosensitivity. *Proc. Natl. Acad. Sci. USA* *101*, 12195–12200.
- S11. Carter, N.J., and Cross, R.A. (2005). Mechanics of the kinesin step. *Nature* *435*, 308–312.
- S12. Paschal, B.M., Shpetner, H.S., and Vallee, R.B. (1987). MAP 1C is a microtubule-activated ATPase which translocates microtubules in vitro and has dynein-like properties. *J. Cell Biol.* *105*, 1273–1282.
- S13. Toba, S., Watanabe, T.M., Yamaguchi-Okimoto, L., Toyoshima, Y.Y., and Higuchi, H. (2006). Overlapping hand-over-hand mechanism of single molecular motility of cytoplasmic dynein. *Proc. Natl. Acad. Sci. USA* *103*, 5741–5745.
- S14. Grill, S.W., Kruse, K., and Julicher, F. (2005). Theory of mitotic spindle oscillations. *Phys. Rev. Lett.* *94*, 108104.
- S15. Howard, J. (2006). Elastic and damping forces generated by confined arrays of dynamic microtubules. *Phys. Biol.* *3*, 54–66.
- S16. Dogterom, M., Kerssemakers, J.W., Romet-Lemonne, G., and Janson, M.E. (2005). Force generation by dynamic microtubules. *Curr. Opin. Cell Biol.* *17*, 67–74.
- S17. Alexander, S.P., and Rieder, C.L. (1991). Chromosome motion during attachment to the vertebrate spindle: Initial saltatory-like behavior of chromosomes and quantitative analysis of force production by nascent kinetochore fibers. *J. Cell Biol.* *113*, 805–815.
- S18. Srayko, M., Kaya, A., Stamford, J., and Hyman, A.A. (2005). Identification and characterization of factors required for microtubule growth and nucleation in the early *C. elegans* embryo. *Dev. Cell* *9*, 223–236.
- S19. Schnitzer, M.J., Visscher, K., and Block, S.M. (2000). Force production by single kinesin motors. *Nat. Cell Biol.* *2*, 718–723.
- S20. Bayas, M.V., Leung, A., Evans, E., and Leckband, D. (2006). Lifetime measurements reveal kinetic differences between homophilic cadherin bonds. *Biophys. J.* *90*, 1385–1395.